An unsteady pressure probe for the measurement of flow unsteadiness in tidal channels

Anna M Young *University of Bath*
Bath, United Kingdom
amy32@bath.ac.uk
Nicholas R Atkins *Whittle Laboratory*
University of Cambridge
Cambridge, United Kingdom
nra27@cam.ac.uk
Christopher J Clark *Whittle Laboratory*
University of Cambridge
Cambridge, United Kingdom
cjc95@cam.ac.uk
Gregory Germain *Ifremer*
Boulogne-sur-Mer, France
Gregory.Germain@ifremer.fr

The work was funded by EPSRC under a SUPERGEN Marine Challenge grant (EP/J010308/1).

Abstract

An unsteady five-hole probe has been developed for the measurement of turbulent flow in tidal channels. Such measurements are vital for accurate prediction of unsteady loads on tidal turbines. Existing field-based velocimeters are either unable to capture the required range of frequencies or are too expensive to profile the variation of turbulence across a typical tidal power site, and thus the available data is inadequate for turbine design.

This work adapts the traditional five-hole wind tunnel probe to achieve a low cost device with sufficient frequency range for tidal turbine applications. The main issue in the marine environment is that the ambient hydrostatic pressure is much higher than the dynamic pressure. This has been overcome by using novel calibration coefficients and differential transducers.

In flume tank tests against LDV measurements, the frequency response of the probe has been shown to be sufficient to capture all the frequencies necessary for tidal turbine design.

Index Terms

Velocity measurement, pressure, multi-hole probe, site assessment, tidal power, turbulence, unsteadiness

NOMENCLATURE

c	Wave propagation speed
f	Frequency
g	Acceleration due to gravity
K_{dyn}	Dynamic pressure calibration coefficient
K_{pitch}	Pitch calibration coefficient
K_{stag}	Total pressure calibration coefficient
K_{yaw}	Yaw calibration coefficient
LDV	Laser Doppler Velocimeter
p	Static pressure
p_0	Stagnation pressure
p_{C}	Centre-hole pressure
p_{D}	Bottom-hole pressure
p_{L}	Left-hole pressure
p_{R}	Right-hole pressure
p_{U}	Top-hole pressure
$\bar{U}$	Bulk flow speed
U_{probe}	Absolute velocity at probe
x	Streamwise co-ordinate
y	Transverse co-ordinate
z	Vertical co-ordinate
ϕ	Pitch angle
θ	Yaw angle

Acronyms

ADCP	Acoustic Doppler Current Profiler
ADV	Acoustic Doppler Velocimeter
CMRR	Common Mode Rejection Ratio

I. Introduction

Tidal turbines operate in a hostile environment - high turbulence levels, waves and large-scale unsteadiness from geographical features combine to generate large fluctuating loads on the turbine blades. Even small errors in unsteady load predictions at the design stage can lead to large reductions in the fatigue life of components. To compound matters, flow conditions can vary considerably even within one site. This means that tidal turbine designers need accurate steady and unsteady flow data across all parts of every potential installation site.

The usual device for measuring tidal flows is the Acoustic Doppler Current Profiler (ADCP), which is chosen for its ease of use - especially the fact that one device can scan across the full depth of the channel while mounted on the seabed. However, it has been shown in previous work by Guion and Young [1] that a standard ADCP cannot capture fluctuations smaller than the radius of a typical turbine (10 m). By contrast, flow structures as small as half a blade chord (0.5 m) are likely to cause unsteady loading issues. The unresolved lengthscales in ADCP data could lead to an under prediction of the unsteady loading and therefore there is the potential for unexpected mechanical failure.

Acoustic Doppler Velocimeters (ADVs) could be used in place of ADCPs as they can capture much smaller flow structures. However, they are less robust than ADCPs and take measurements at a single location, meaning that multiple devices are required to give information about flow variation with depth. Furthermore, both devices are too expensive to deploy at more than a few locations across a site. There is, therefore, a need for a low cost, easily deployable device that can capture unsteady velocity fluctuations with lengthscales of the order of half a blade chord. Given the bulk convection speeds found in typical tidal channels, this translates to a minimum frequency response of approximately 10 Hz.

The use of multi-hole pressure probes is commonplace in conventional turbomachinery research. For applications where space constraints are not too onerous, fast-response versions have been developed with the sensing components built into the probe head. Most recently, a fast-response five-hole probe has been developed by Duquesne, Deschênes, Iliescu, and Ciocan [2], and tested in small-scale, low hydrostatic head water pumps by Duquesne, Ciocan, Aeschlimann, Bombenger, and Deschênes [3]. The major difference between their work and the application discussed here is the background hydrostatic pressure, which is negligible in a small water pump, but will be up to two orders of magnitude larger than the dynamic pressure in a typical tidal

channel. The hydrostatic pressure at depth in a tidal channel therefore dwarfs any changes in pressure due to unsteady flow passing over the sensors.

Similarly, in a wind tunnel, the atmospheric pressure will be much larger than the dynamic pressure, but this issue is overcome by using differential sensors with one side measuring a reference such as the tunnel inlet pressure or the laboratory atmospheric pressure. The marine environment, however, does not offer a convenient 'reference' pressure.

The prior art in the area of multi-hole pressure probes therefore suggests that the technology could be transferred into the marine environment in order to provide unsteady flow measurements if the high hydrostatic pressure can be accommodated without sacrificing accuracy. One solution to the lack of reference pressure is to use differential measurements; this is the approach taken in the work presented here.

This paper discusses the development of a marine five-hole probe. A prototype has been manufactured and benchmarked against an LDV reference system in the flume tank at Ifremer, Boulogne-sur-Mer, France. In the tests at Ifremer, the probe was shown to capture frequencies up to 20 Hz accurately - more than sufficient for the calculation of unsteady loads on a tidal turbine.

After an introduction to multi-hole probes (Section II), the key differences between tidal channel flows and those encountered in wind tunnel testing will be discussed in Section III. The novel calibrations required for taking measurements at depth will be derived in Section IV. After this, key aspects of the probe design will be outlined in Section V, and the test setup will be explained in Section VI. The calibration of the prototype probe will be described in Sections VII and VIII. The steady flow accuracy and unsteady frequency response will then be discussed in Sections IX and X, respectively, before improvements are discussed and conclusions drawn.

II. Multi-hole pressure probes

Multi-hole probes are commonly used in aerospace applications to make point measurements of flow angles along with static and stagnation pressure. A section through a typical probe head is shown schematically in Fig. 1. The centre, left and right holes are shown. On the left-hand diagram, the probe is aligned with the flow; this means that the left and right holes will give equal pressure readings, and the centre hole will register the stagnation pressure of the flow. If the flow is at an angle to the probe, as shown on the right-hand diagram in Fig. 1, one of the

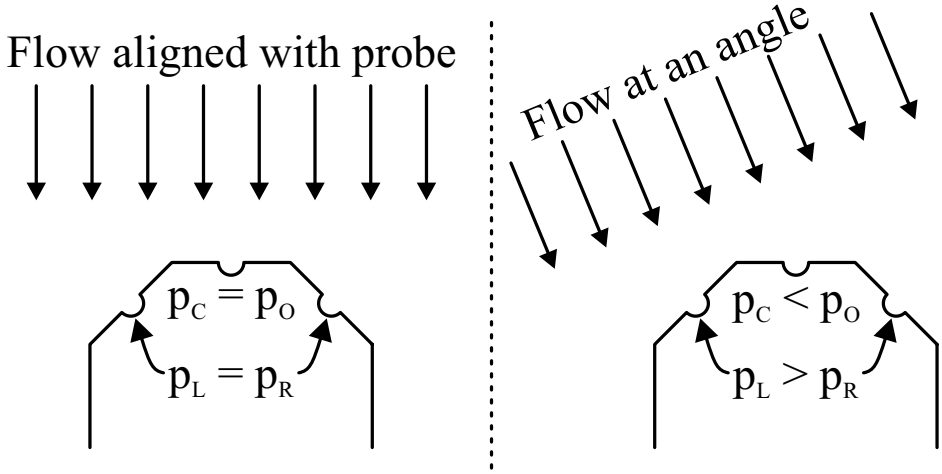

Fig. 1. Principles of operation of a five-hole probe.

side holes will read a higher pressure than the other, and the centre hole will no longer give the stagnation pressure.

By acquiring data with the probe at different yaw and pitch angles in a known, uniform flow, calibration maps can be generated, which give the relationship between flow direction and the relative hole pressures. The most commonly-used calibration coefficients, K, are:

$$K_{\text{yaw}} = \frac{p_{\text{L}} - p_{\text{R}}}{p_{\text{C}} - \frac{1}{4}\left(p_{\text{L}} + p_{\text{R}} + p_{\text{U}} + p_{\text{D}}\right)} \tag{1}$$

$$K_{\text{pitch}} = \frac{p_{\text{U}} - p_{\text{D}}}{p_{\text{C}} - \frac{1}{4}\left(p_{\text{L}} + p_{\text{R}} + p_{\text{U}} + p_{\text{D}}\right)} \tag{2}$$

$$K_{\text{dyn}} = \frac{p_0 - p}{p_{\text{C}} - \frac{1}{4}\left(p_{\text{L}} + p_{\text{R}} + p_{\text{U}} + p_{\text{D}}\right)} \tag{3}$$

$$K_{\text{stag}} = \frac{p_0 - p_{\text{C}}}{p_{\text{C}} - \frac{1}{4}\left(p_{\text{L}} + p_{\text{R}} + p_{\text{U}} + p_{\text{D}}\right)} \tag{4}$$

where p_{L}, p_{R}, p_{U}, p_{D} and p_{C} are the pressures recorded on the left, right, up, down and centre holes, respectively, p_0 is the flow stagnation pressure, and p is the flow static pressure.

The calibration maps derived from a known flow can be applied to data acquired in a wind tunnel test or in the aero-engine environment: the raw pressures from each hole are used to find K_{yaw} and K_{pitch}, and the calibration map is then inverted to find the yaw angle, θ, the pitch angle, ϕ, and therefore K_{dyn} and K_{stag}. Assuming incompressible flow, the velocity of the flow onto the probe is given by:

$$U_{\text{probe}} = \sqrt{\frac{K_{\text{dyn}}\left(p_{\text{C}} - \frac{1}{4}\left(p_{\text{L}} + p_{\text{R}} + p_{\text{U}} + p_{\text{D}}\right)\right)}{\frac{1}{2}\rho}} \tag{5}$$

The streamwise, transverse and vertical velocity components are then found by converting from spherical polar to Cartesian co-ordinates:

$$U_{\mathrm{x}} = U_{\mathrm{probe}} \cos\phi \cos\theta \tag{6}$$

$$U_{\mathrm{y}} = U_{\mathrm{probe}} \cos\phi \sin\theta \text{ , and} \tag{7}$$

$$U_{\mathrm{z}} = U_{\mathrm{probe}} \sin\phi \tag{8}$$

At high yaw/pitch angles (usually around 30° to 45°), the flow on one of the faces of the probe will separate; this causes a sharp drop in pressure on one face. The behaviour of the probe when the flow is separated can be highly dependent on Reynolds number, so researchers usually aim to use their probes only within the unseparated range, and it is preferable to 'null' the probe such that the side face pressures are equalised before measurements are taken, instead of relying on the accuracy of the extreme edges of the calibration map. This approach cannot, however, be taken in an unsteady flow environment, and so various adjustments to the calibration coefficients can be made to increase the accuracy of data at high angles [4].

III. Size and scale considerations

The typical ranges of conditions in tidal channels are compared with those encountered in aerospace applications in Table I (supersonic and hypersonic facilities are ignored in this analysis). It can be seen that the increase in density between air and seawater is offset by much lower flow speeds in the sea, such that the dynamic pressures expected in a tidal channel are comparable with the low speed end of typical wind tunnel test facilities. This, along with the blade Reynolds numbers being in the same range, suggests that similar measurement techniques will be appropriate for both flows. However, there are some major differences between the two applications: hydrostatic pressure, unsteady flow lengthscales and probe Reynolds number.

The main differences in measurement requirements between aero-engines and marine channels will now be discussed in turn.

A. Pressures

The hydrostatic pressure at 20 m depth (the hub height of a typical 1 MW turbine) will be almost 200 kPa, which is between 45 and 400 times larger than the dynamic head of the flow.

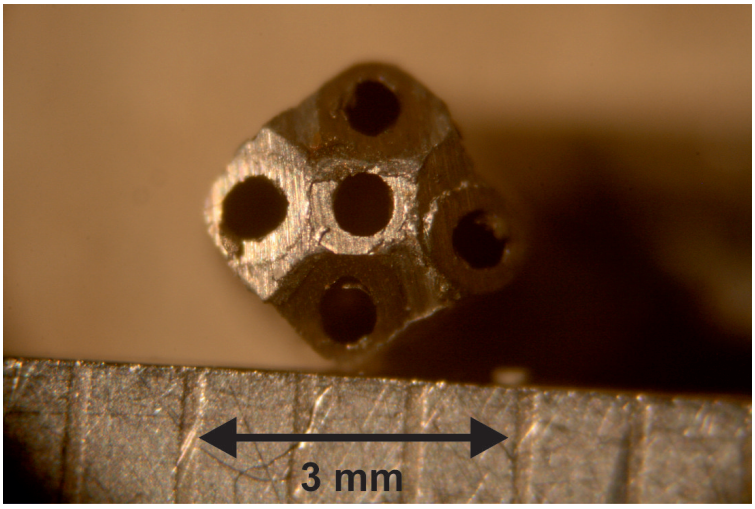

Fig. 2. Typical five-hole probe for wind tunnel applications (photo courtesy of James Taylor).

In order to measure the flow speed accurately, the dynamic pressure must therefore be isolated from the hydrostatic pressure prior to measurement.

In wind tunnel testing, the atmospheric pressure is also far higher than the dynamic pressure, and the issue of transducer sensitivity is solved by using differential sensors which are all connected to the local atmospheric pressure (or the tunnel inlet static pressure). This straightforward technique allows sensors with a full-scale range similar to the dynamic head to be used, as opposed to absolute transducers which would not be able to capture small changes in flow speed.

Differential pressure transducers with full-scale range similar to the dynamic head are thus essential in both wind tunnel and marine applications. There is, however, no convenient 'reference' pressure in the marine environment at depth and so the pressures on the probe faces must be measured relative to one another. The exclusive use of differential transducers without an independent reference pressure necessitates a novel set of calibration coefficients, which will be discussed in detail in Section IV.

B. Unsteady Flow Lengthscales and Frequencies

In wind tunnel testing, researchers are usually interested in high-frequency, small-scale flow features related to loss generation. In tidal turbine design, however, the major need is to capture the unsteady flow structures in the channel. This means that the scales of interest are vastly different in the two applications, as shown in Table I.

158 A tidal turbine designer needs information on unsteady flow structures down to scales equiv-
159 alent to half the turbine chord in order to predict unsteady loading. This means that the flow
160 features of interest range in size from 500 mm to 35 m. This makes it easier to manufacture a
161 robust device and to mount the pressure transducers directly on the probe faces.

162 While miniature, high-frequency pressure transducers are generally manufactured to order in
163 small batches, larger transducers with a lower frequency response are mass-produced for a wide
164 range of applications. This therefore allows the use of lower cost components in the marine
165 probe than in aerospace versions.

166 A further advantage of the large size of the probe is that geometric variation due to man-
167 ufacturing tolerances will have a negligible impact on the calibration map. Work by Hall and
168 Povey [5] has shown that, for a probe produced using additive manufacturing, the calibration
169 map is unaffected by geometric defects due to tolerances as long as the probe diameter is above
170 4 mm. This means that, for probes of the type discussed in this paper, individual devices would
171 not have to be calibrated. Once a map of the type shown in Section VIII was produced for
172 a given design, it would be universally applicable to all probes. This would drastically reduce
173 costs, as performing a full yaw and pitch calibration for every device is a lengthy process[1].

174 *C. Probe Reynolds number*

175 The Reynolds number of the probe developed in this work (75 mm diameter) is compared
176 with that of typical aerospace probes in Table I. It can be seen that there is an overlap in
177 the range of Reynolds numbers experienced in the two applications. Work by Dudzinski and
178 Krause [6] on fixed orientation probes, and their sensitivity to Reynolds number, showed that in
179 some circumstances the probe must be calibrated at a series of different Reynolds numbers in
180 order to obtain accurate data.

181 Building on this work, Dominy and Hodson [7] undertook a series of tests with different probes
182 and at varying flow speeds. They found that the calibration map was approximately independent
183 of Reynolds number when the probe Reynolds number was above 15×10^3, which is 5 times less
184 than the Reynolds number of the prototype probe discussed here. Their work therefore means
185 that the prototype probe developed here is expected to give readings that are independent of
186 Reynolds number. This will be examined in Section VI.

[1]The electronic components will still need calibration, as outlined in Section VII, but this is a far quicker, cheaper process than the yaw and pitch calibration

TABLE I

COMPARISON OF FLOW PROPERTIES FOR TIDAL AND WIND TUNNEL APPLICATIONS.

Quantity	Tidal	Wind tunnel
Working fluid		
Density (kg/m^3)	997	1.225
Kinematic viscosity (m^2/s)	1.0×10^{-6}	1.6×10^{-5}
Flow speed (m/s)	$1-3$	$30-300+$
Reynolds numbers		
Typical blade chord (m)	1	0.05
Typical blade Reynolds number	$1-3\times10^6$	$0.1-1\times10^6$
Typical probe diameter (mm)	75	$1-10$
Typical probe Reynolds number	$75-230\times10^3$	$2-100\times10^3$
Pressures		
Depth (m)	$10-80$	n/a
Hydrostatic pressure (gauge, kPa)	$99-790$	n/a
Dynamic pressure (p_0-p, kPa)	$0.49-4.5$	$0.55-55$
Lengthscales		
Flow lengthscales of interest	$0.5-35$ m	$1-50$ mm
Max. frequency of interest (Hz)	10	50000+
Kolmogorov microscale (μm)	$50-100$	$1-8$

IV. NEW CALIBRATION COEFFICIENTS

In order to overcome the twin issues of high ambient hydrostatic pressure and a lack of a local reference pressure, differential transducers must be used between the probe faces. This, in turn, requires a novel set of calibration coefficients. Each transducer measures the difference in pressure between the centre hole and one of the four side holes. Using these novel coefficients, the yaw and pitch angles can be calculated as with a conventional probe, and the dynamic pressure can be found. It can be seen that the conventional yaw coefficient:

$$K_{\text{yaw}} = \frac{p_{\text{L}}-p_{\text{R}}}{p_{\text{C}}-\frac{1}{4}\left(p_{\text{L}}+p_{\text{R}}+p_{\text{U}}+p_{\text{D}}\right)} \tag{9}$$

can be obtained using differential signals via the following mathematically equivalent expression:

$$K_{\text{yaw}} = \frac{(p_{\text{C}}-p_{\text{R}})-(p_{\text{C}}-p_{\text{L}})}{\frac{1}{4}\left[(p_{\text{C}}-p_{\text{L}})+(p_{\text{C}}-p_{\text{R}})+(p_{\text{C}}-p_{\text{U}})+(p_{\text{C}}-p_{\text{D}})\right]} \tag{10}$$

Similar expressions for the pitch coefficient, K_{pitch}, and the dynamic coefficient, K_{dyn}, can also be found:

$$K_{\text{pitch}} = \frac{(p_{\text{C}} - p_{\text{D}}) - (p_{\text{C}} - p_{\text{U}})}{\frac{1}{4}\left[(p_{\text{C}} - p_{\text{L}}) + (p_{\text{C}} - p_{\text{R}}) + (p_{\text{C}} - p_{\text{U}}) + (p_{\text{C}} - p_{\text{D}})\right]} \tag{11}$$

$$K_{\text{dyn}} = \frac{p_0 - p}{\frac{1}{4}\left[(p_{\text{C}} - p_{\text{L}}) + (p_{\text{C}} - p_{\text{R}}) + (p_{\text{C}} - p_{\text{U}}) + (p_{\text{C}} - p_{\text{D}})\right]} \tag{12}$$

As shown in Section II, the calibration map can be inverted to find the pitch and yaw angles and then the flow speed can be derived from the dynamic coefficient and Bernoulli's equation (as the flow is incompressible). The total pressure coefficient, however, cannot be derived from the differential measurements available. This means that the absolute static and stagnation pressures cannot be found (unless an additional, absolute transducer is fitted). This is not of concern in the current work, as the quantities of interest are flow speed and direction, for which the yaw, pitch and dynamic coefficients are sufficient.

V. Proof of Concept Prototype

The prototype probe is shown schematically in Fig. 3(a). The probe diameter is 75 mm and the distance from the front of the probe to the right-angle in the stem is approximately three diameters. The prototype was built using low-cost commodity components and rapid-prototyped parts.

Unlike a wind tunnel probe, the marine device has to survive in a corrosive fluid (sea water) at high pressure. The probe in Fig. 3 was made from four parts which were 3D printed using a polymer with similar properties to ABS or polypropylene (depending on the life-span required, production models could be machined from marine-grade stainless steel).

It can also be seen from Fig. 3(a) that the prototype has a conventional five-hole probe head, with two design features suggested by Dominy and Hodson [7]. Firstly, the faces are at 45^{o} to one another and have sharp edges. This design gives superior performance to a cone-type probe at high yaw and pitch angles. Secondly, the holes are perpendicular to, and at the centre of, each face - moving the holes back from the front edge reduces the effect of Reynolds number on the probe calibration map. Ainsworth, Allen and Batt [8] found that the optimal hole position is not necessarily at the centre of the face. However, the holes are central on the prototype for ease of construction.

An internal section view of the probe is given in Fig. 3(b). It can be seen that the device has on-board amplification and that there is sufficient space within the body for on-board data

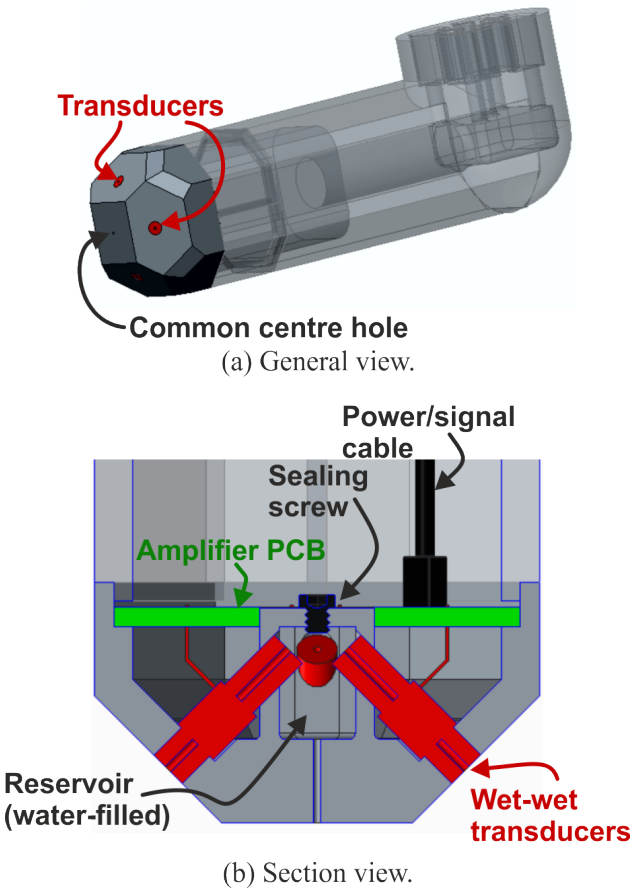

(a) General view.

(b) Section view.

Fig. 3. Drawing of probe head design and transducer location.

acquisition and a battery, as is common in marine measurement devices. For the purpose of this test, however, a standard laboratory grade data acquisition system was used, mounted immediately above the water surface, connected to the probe by 3 m cables and controlled by a desktop PC. The electronic components are protected from exposure to water, with the exception of the transducers, which are wet-wet and are exposed to water on both sides of their diaphragms.

The pressure sensors (shown in red) are low-cost commercial-off-the-shelf wet-wet differential transducers with a full scale range of 7 kPa (to the authors' knowledge, this was lowest range wet-wet transducer available with sufficiently small dimensions). Although 7 kPa is appropriate for a typical tidal channel flow, the flume tests were run at 0.8 m/s, which is at the low end of expected field conditions. As a result, the peak dynamic head in the flume is only about 0.5 kPa. In addition, the transucers have a full scale output of 16.7 mV, which is relatively low. In order to generate usable data from such small signals, a low noise, high CMRR instrumentation amplifier

(shown in green) was fitted within the probe head. The amplifier had a differential gain of 200, and a line driver was incorporated into a custom PCB which was fitted immediately behind the transducers.

The transducers are mounted directly in the holes on the faces, with the minimum possible tube length between the probe face and the sensing diaphragm. The four rear ports of the transducers are immersed in a reservoir which is connected to the centre hole of the probe. This means that each transducer will measure the difference between the centre hole and one of the side holes, thus eliminating the hydrostatic pressure as described in Section IV.

Not shown in Fig. 3 are the reference thermocouples, which are used to provide temperature compensation for the pressure transducers, and a copper heat sink which ensures constant temperature across the probe head even if there is a temperature gradient in the flow.

As water is considered incompressible, the reservoir should have a negligible effect on the frequency response over the range of frequencies and pressures considered here. However, the presence of an air bubble anywhere between the probe faces and the transducer diaphragms is likely to introduce a resonant response. In order to prevent this, the centre hole was sealed temporarily, and the probe orientated with the centre hole facing downwards. Whilst in this configuration, the reservoir and the transducer ports were filled with water using a syringe. This process was repeated over a period of several hours to allow air bubbles to rise to the surface.

Once the reservoir was full and free of air bubbles, the sealing screw was inserted and the centre hole was re-opened at the same time to prevent overpressure. The front ports of the transducers were also filled with water in a similar manner. Care was taken to keep the reservoir and ports full during transit and installation.

The impact of an air bubble in the reservoir on the frequency response can be estimated by considering the pressure ports and reservoir as Helmholtz resonators. The corresponding resonant frequencies are given in Table II. It can be seen that, for the ideal case, where the reservoir and the port are both completely filled with water, the Helmholtz resonance frequency is 20 kHz, which is 3 orders of magnitude higher than the frequencies of interest. Introducing even a small air bubble, however, reduces the resonant frequency considerably. The worst-case scenario is when the port is completely water-filled, but the reservoir is completely air-filled. This gives a resonant frequency of 16 Hz. From the information in Table II, it can be seen that the resonant frequency will be higher than 50 Hz as long as the reservoir is at least 90% filled with water. This is achievable with the method described above.

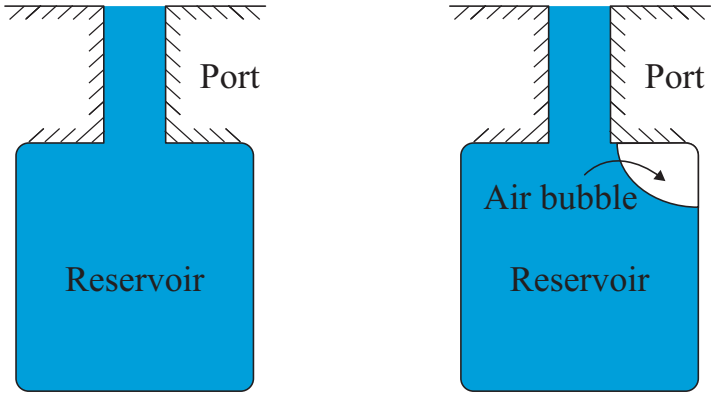

(a) Ideal scenario.

(b) Potential location of air bubble.

Fig. 4. Pressure port and reservoir as a Helmholtz resonantor with and without air bubble.

TABLE II

HELMHOLTZ RESONANCE FREQUENCIES FOR PORTS AND RESERVOIR WITH DIFFERENT LEVELS OF WATER.

Percentage of reservoir filled with water	Percentage of port filled with water	Helmholtz frequency (Hz to 2 s.f.)
100	100	20000
0	0	470
0	100	16
50	100	23
70	100	30
80	100	36
90	100	51
95	100	73
98	100	110

VI. TEST SETUP

The probe was tested in the flume tank at Ifremer, Boulogne-sur-Mer, France. The flume has a working section which is 2 m deep by 4 m wide and a background turbulence level of approximately 5%. The tank is equipped with wave maker paddles for combined wave and current testing. The maximum nominal flow speed is 1.6 m/s with clean flow and 0.8 m/s with waves.

Measurements from the reference LDV system (see below) showed that the mean speed was controlled to within $\pm 1\%$ of the nominal flow speed without waves. It is known that the flow is

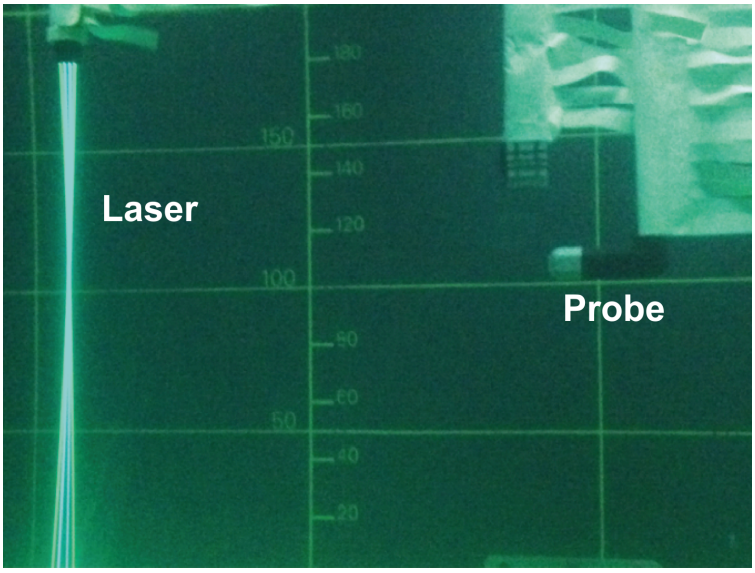

Fig. 5. Test setup in flume tank at Ifremer with LDV upstream of prototype probe.

slightly faster at mid depth when waves are being generated (see [9]), and this can be seen in Fig. 11, where the nominal flow speed is 0.8 m/s but the probes are both measuring an average flow speed of 0.9 m/s. For further details of the test facility and the uniformity of the flow in the test section with and without waves, see [9] and [10].

A photo of the test setup is shown in Fig. 5. The probe was fitted centrally at mid-depth in the flume and tested in flow speeds of 0.4 to 1.6 m/s in clean flow, and at 0.8 m/s with 0.5 Hz surface waves (100 mm wave height).

A. Probe Setup

The probe-holder was designed such that the probe head could be yawed from -45° to +45°, but mounting constraints meant that the pitch angle could only be adjusted to three levels (0, 6.3° and 12.2°). This allowed a full yaw calibration to be undertaken and a limited pitch calibration. A probe of this size is expected to be symmetrical, as manufacturing errors will be negligible, and so the only asymmetry is expected to be in the pitch direction. This asymmetry will be due to the effect of the probe stem (which may divert the flow and thus induce a slight pitch angle onto the probe), and due to the difference in hydrostatic pressure between the top and bottom holes (which is approximately 500 Pa for the probe tested here). This asymmetry will be discussed in Section VIII.

297 In order to compare the calibration with the expected behaviour of the probe, the data will be
298 compared with two models. First, results will be used from a RANS simulation of the probe head
299 (i.e. without the stem) at pitch and yaw angles from -20° to +20°. Second, the inviscid model
300 of Zilliac [11] will be plotted, using the streamline projection method of Chondrokostas [12].
301 The unsteady data shown in this paper is from 240-second long samples; this corresponds to
302 approximately 20 tank through-flow times. The sample rate for the probe was set to 10 kHz in
303 order ensure that the data was over-sampled and to allow for filtering at a later point.

304 *B. Flow Reference Measurements*

305

306 In all tests, a Laser Doppler Velocimeter (LDV) was set up 2.5 m upstream of the probe and
307 data acquisition was undertaken simultaneously so as to provide reference measurements. The
308 LDV system could only record the axial and transverse velocity components, while the five-hole
309 probe recorded all three velocity components (axial, transverse and vertical). In a separate test,
310 the LDV was repositioned and the vertical component of the flow was measured with waves.
311 The LDV system available at Ifremer is 2 dimensional, i.e. composed of 4 laser beams with
312 2 different wave lengths: 514 nm and 488 nm. The measurement volume is 2.51 mm long and
313 the laser beam thickness is 0.12 mm (giving a volume of 0.01 mm^3). This is a smaller sampling
314 volume than that of the probe, where it is assumed that the flow is uniform over the probe head
315 (75 mm in each direction). This difference in sampling volume should not be an issue for the
316 work presented here because the fluctuations in the flow are negligible over lengthscales of the
317 size of the probe head.
318 The water in the tank is seeded with particles of silver-coated glass with a typical diameter
319 of 10 μm; this should be small enough to follow the flow, yet large enough to scatter sufficient
320 light to obtain a good signal-to-noise ratio.
321 The mean sample rate of the LDV was 540 Hz in the axial direction and 240 Hz in the
322 transverse direction, but this rate varied in both directions due to the random rate at which
323 particles crossed the sample volume.
324 In order to compute the power spectral density and autocorrelation of the LDV data, it is
325 usually necessary to re-sample at a constant sample rate. The LDV spectra shown here have
326 been computed by using a zeroth-order sample and hold technique, as advocated by Tropea and
327 Yarin [13], with the re-sampling rate set to the minimum LDV sample rate (approximately 50 Hz

in the streamwise direction and 20 Hz in the transverse direction), in order to avoid artificial alterations to the spectra obtained.

VII. Transducer Calibration and Drift

The pressure transducers mounted in the probe head give an analogue signal in Volts. This signal is recorded via an Analogue-to-Digital converter and must then be converted into pressure in Pascals before the calibration coefficients described in Section VIII are used to find the flow speed and direction. For the transducers used in this study (Omega PX26 wet-wet differential sensors), pressure and voltage should be related linearly:

$$P = A\,(V - V_0) \tag{13}$$

where P is the pressure on the probe face, V is the voltage given by the transducer, A is the calibration gradient (given in Pascals per Volt) and V_0 is the voltage recorded when there is no pressure difference across the transducer. The zero-pressure voltage is determined by the error in resistance of the resistors making up the Wheatstone bridge circuit inside the transducer, and will change with temperature. The effect of temperature on V_0 and the calibration gradient, A, will now be shown.

The effect of temperature on the zero-pressure voltage, V_0, is shown in Fig. 6(a). Results for two transducers are shown, to illustrate the variability between sensors. It can be seen that the zero offset varies from one transducer to the next, and that changing the temperature of the transducer creates an approximately linear change in the zero-pressure voltage. In an environment where temperature changes were expected, the thermocouples in the probe head could be used to correct the readings. In all the results shown in this paper, the zero level was measured at the start and end of each experiment and the temperature changes were negligible during any given experiment (< 0.2°C). The flow speed was found to have no effect on the temperature measured inside the probe head.

Figure 6(b) shows the response of the same two sensors to changes in pressure (both positive and negative) at two temperatures. The maximum pressure used (450 Pa) is the dynamic head of water flowing at 1.0 m/s (i.e. far smaller than the range of the sensors, which is 6700 Pa). Considering first the calibrations at 16°C (black and red lines), it can be seen that the calibration gradients are slightly different between the two sensors, and that sensor 1 has a more linear response than sensor 2 (the black squares lie closer to the linear fit line than the red squares).

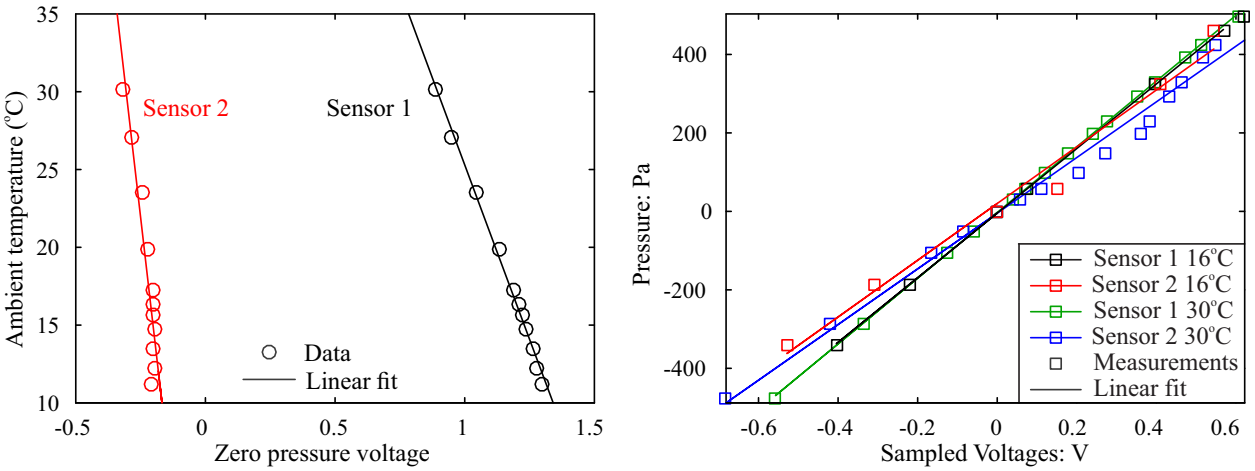

(a) Effect of temperature on zero-pressure voltage.

(b) Pressure against voltage at two temperatures.

Fig. 6. Pressure transducer calibration (two sensors shown).

When the calibration was repeated at 30°C (green and blue lines), more points were recorded in the range near zero pressure. Two things can be observed: first, there is little or no change in the calibration gradient with temperature. Second, sensor 2 shows significant non-linearity over the range 0-200 Pa. This is a departure from the ideal behaviour but is within the manufacturer's specification and highlights the issues arising when sensors are used over only 10% of their specified range. The calibration applied to the data to convert from voltage to pressure can be adapted to account for this non-linearity, or higher accuracy transducers can be used.

Not considered here are any effects on the calibration of a common-mode offset caused by the transducer being at depth. This may change both the zero offset and the calibration gradient of the transducers. In the tests shown below, the zero levels of the transducers were measured with the probe installed in the flume tank, to minimise any common-mode errors.

VIII. Steady Flow Yaw and Pitch Calibration

The second stage in the calibration process is to convert the four differential pressure measurements ($p_C - p_L$, $p_C - p_R$, $p_C - p_U$ and $p_C - p_D$) into flow speed and direction using the calibration procedure described in Section IV. In order to do this, the calibration coefficents must be recorded at different yaw and pitch angles to produce a calibration map. The map will be discussed in this section.

The calibration coefficients are shown in Fig. 7(a) as a function of yaw angle for tests with flow speeds of 0.8 m/s and 1 m/s, and as a function of pitch angle in Fig 7(b). The calibration

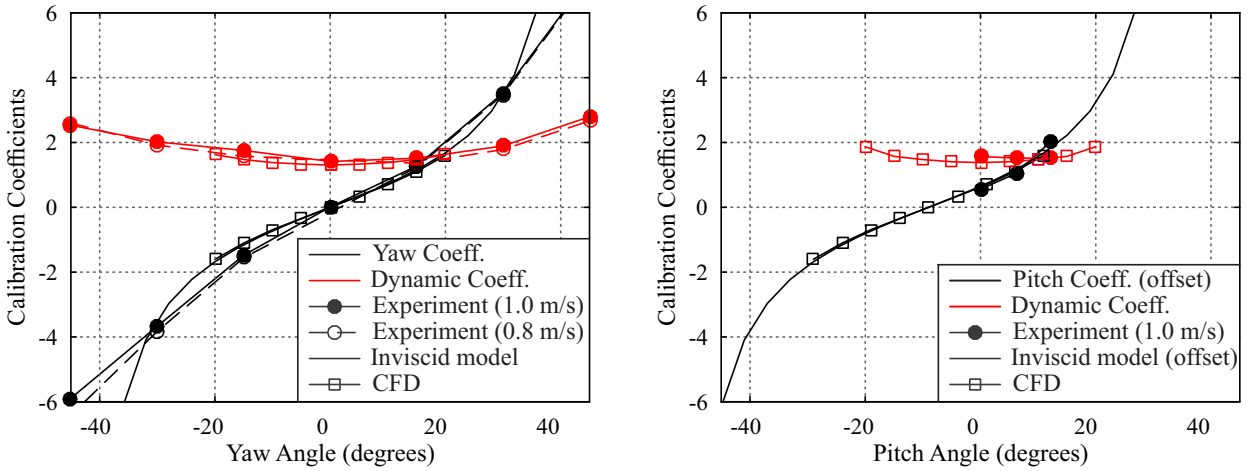

(a) Effect of yaw on calibration coefficients (0° pitch). (b) Effect of pictch on calibration coefficients (0° yaw).

Fig. 7. Calibration coefficients against yaw and pitch angle.

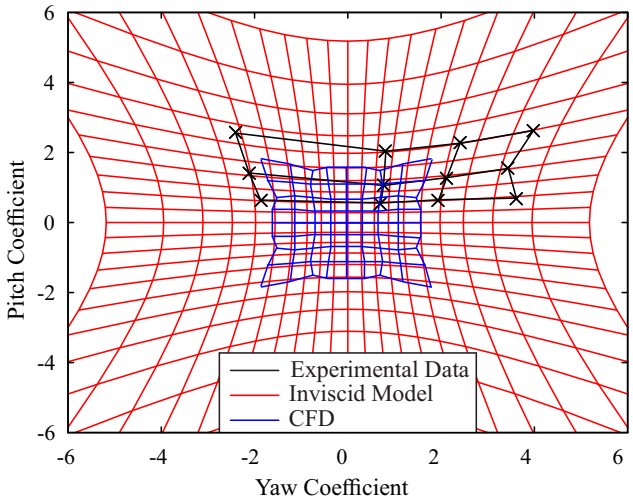

Fig. 8. Pitch coefficient against yaw coefficient (1.0 m/s flow speed).

data (large circles) is compared with a set of RANS CFD solutions for the probe (squares) and against the inviscid, analytical solution of Zilliac [11] (using the streamline projection method of Chondrokostas [12]) for yaw and pitch coefficient (solid lines).

It can be seen that the probe behaves as expected: the dynamic pressure coefficient is approximately constant for angles less than $\pm 20^{\circ}$, while the yaw coefficient is linear over the same range. There is good agreement between the experimental data, the CFD and the analytical solution over smaller angels. At larger yaw angles, separation on whichever face is at the most extreme angle to the flow causes the coefficients to deviate. This causes disagreement between

the inviscid model and the probe data at yaw angles of $\pm 45°$.

Constraints in the experimental setup meant that it was only possible to test the probe at three different pitch angles: 0°, 6.3° and 12.2°. The pitch coefficient is not zero at zero pitch. This is due to the effect of the probe stem meaning that the probe records a pitch coefficient equivalent to 9° of pitch at zero degrees. In Fig. 7(b), the CFD and analytical solutions for pitch coefficient have been shifted by 9° to account for these effects. As with the yaw angle behaviour, the agreement between the experiment and the models is good and the pitch and dynamic coefficients follow the expected trends.

The hydrostatic pressure gradient in water $\left(\frac{\partial P}{\partial z} = \rho g\right)$ is approximately 9800 Pa/m, giving a difference in pressure between the top and bottom holes of approximately 500 Pa (and this head difference will be identical inside the probe assuming a water-filled reservoir). In the results shown here, this has been accounted for in the zero-flow voltage measurements taken at the start of each experiment. In a tidal channel, where the hydrostatic pressure gradient will vary with temperature, depth and salinity, an additional differential measurement could be used to find the local gradient.

Another way to visualise the calibration coefficients is to plot the pitch coefficient against yaw coefficent so that the combined effect of yaw and pitch can be seen. This has been done in Fig. 8. The red grid shows the results from the inviscid model, while the CFD calculations are shown in blue and the black crosses show the experimental data. It can be seen that the agreement between the two models and the experiments is good.

Returning to Fig. 7(a), there is very little variation between the yaw and dynamic coefficent curves for the two flow speeds. This suggests that Reynolds number effects are minimal (at least over the speed range tested here). This is in line with the findings of Dominy and Hodson [7], who showed that Reynolds number effects are only important for probe Reynolds numbers below 15×10^3, far lower than the Reynolds numbers in typical tidal channels (see Table I).

The best way to minimise errors due to Reynolds number sensitivity and data uncertainty is to avoid using the probe at high angles of attack where one face is separated. This is usually achieved by 'nulling' the probe such that it faces the bulk flow direction.

In situations where this is not possible - due to high levels of unsteadiness, or the probe being fixed (both of which will be true in a tidal channel) - the angle range of the probe can be improved by changing the denominator of the calibration coefficients. There are numerous permutations in the literature, including those of Dunkley [4], who used a weighting factor to

bias the denominator towards the holes which were closest to the local stagnation pressure.

IX. Accuracy of Steady Velocity Measurements

The calibration from above can now be applied to measured data to assess the accuracy of the probe. The test data used for this purpose is from a series of tests at seven different flow speeds from 0.4 m/s to 1.6 m/s and from six independent tests at 0.9 m/s. Measurements were averaged over tens of thousands of samples so that the precision error is negligible, and the errors found will be the cumulative bias error from the transducer measurement and the calibration map.

The main error is expected to be from the transducer bias error, which is quoted by the manufacturer as 1% of full scale (i.e. 69 Pa or 15% of the dynamic head in water at 1.0 m/s). This bias error can be reduced by calibrating each transducer as described in Section VII. This process will eliminate errors due to variations in sensitivity or linearity, and will account for the dependence of zero pressure voltage on temperature. Any drift in the zero level during tests will, however, introduce significant errors and it will be shown that this drift dominates the total error.

Prior to the accuracy tests discussed here, it was found that there was an offset between the measured probe velocity and the true flow speed. This was corrected by applying a voltage offset of 25 mV to the zero level of each transducer, both for the calibration described above and for the data shown in Figs. 9 and 10 (i.e. $P = A\left(V - V_0 + 0.025\right)$). The reasons for this offset are unclear, but it appears that the zero pressure voltage changes when the flume tank is switched on (there is no change in temperature, so it is not due to a lack of temperature compensation).

Figure 9 shows measured velocity against true flow velocity from tests at seven different flow speeds. The red line represents zero error, while the blue dashed lines show error bands of $\pm 5\%$. The red dots are the data, to which a zero level offset of 25 mV has been applied as described above. It can be seen that all the red dots lie within the 5% error band, with the exception of the 0.4 m/s case. This gives a lower bound on the flow speeds that can be measured with the probe, as the dynamic head becomes too small to record accurately ($P_0 - P$ is approximately 450 Pa at 1 m/s and only 72 Pa at 0.4 m/s).

The errors in measured flow speed for six independent tests at 0.9 m/s are shown in Fig. 10. Tests 1-4 were undertaken with waves present at 0.5 Hz, while tests 5-6 were undertaken in clean flow. Again, an offset of 25 mV has been applied to the measured zero pressure voltage. It can be seen that the scatter in the data is small (less than 2% of the mean flow speed), but that

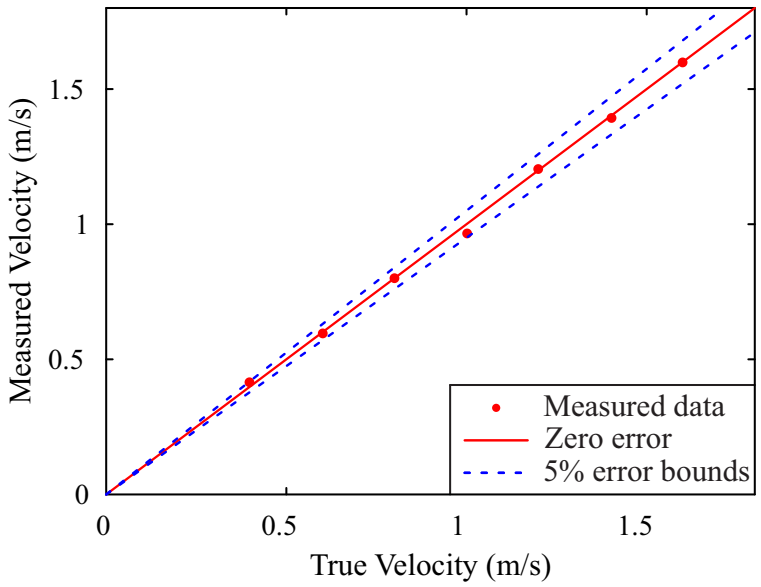

Fig. 9. Measured flow speed against actual flow speed (with corrected zero levels).

there is an offset of 5-10% in the flow speed. Applying a further offset of 12 mV to the data gives the red dots - all within $\pm 1\%$ of the real flow speed ((i.e. $P = A\,(V - V_0 + 0.037)$). Once again, transducer drift is the main source of the error in the steady flow velocity measurements.

From this data, it can be concluded that the errors in mean flow speed are due to drift in the zero-pressure voltages given by the transducers. The offset in the zero level is not understood, as zero levels were recorded immediately prior to running the experiments and there was no appreciable temperature change. The data also shows that the lower bound of speeds which can be measured to $\pm 5\%$ is 0.6 m/s. Using higher specification transducers would improve the steady flow accuracy of the probe; the problem shown here is not inherent to the probe design.

X. Unsteady Flow Measurement Comparison

The main aim of this work is to show that the probe can resolve unsteady flow features of the scales relevant to tidal turbine designers (0.5 to 35 m, or frequencies up to 10 Hz). This will be shown now with data taken from the probe and the reference LDV described in Section VI-B both with and without waves.

Constraints in the flume tank mounting arrangement mean that there was a spatial offset (2.5 m) between the LDV and the probe. This offset means that it is necessary to shift the signals in time in order to compare unsteady velocity measurements. However, different flow structures

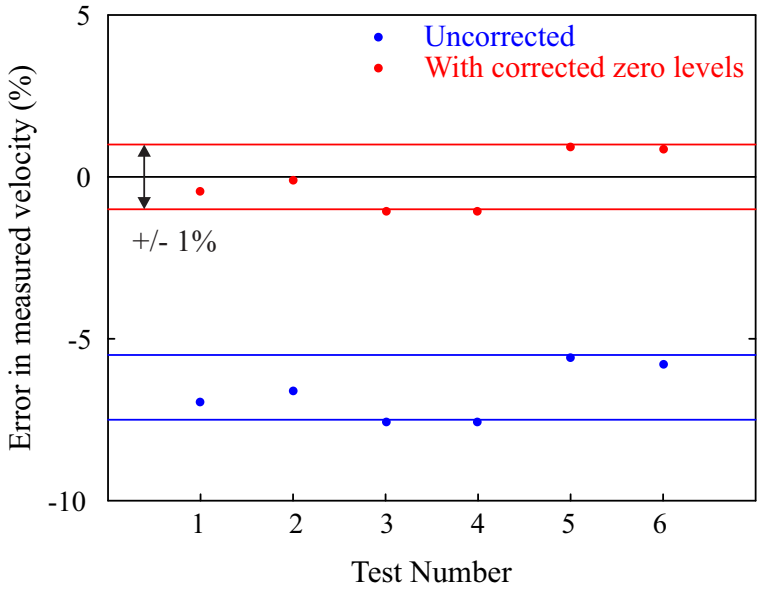

Fig. 10. Error in measured flow speed from six tests at 1.0 m/s with and without zero level correction.

will convect at different speeds and so it is not possible to compare all flow structures directly between the two measurements. The two primary speeds at which structures may convect are the bulk flow speed, $\bar{U}$, and the speed of the surface waves, which is given by:

$$c = \bar{U} \pm \frac{g}{2\pi f} \tag{14}$$

where f is the frequency of the waves. The propagation speeds of other structures are unknown, and new small structures are likely to evolve between the two measuring locations.

A comparison of the streamwise flow velocity from the two devices is given in Fig. 11 (a), with a temporal shift (based on the wave propagation speed) applied to account for the spatial offset between probes. The data shown is from a test at 0.8 m/s with waves at 0.5 Hz. In order to enable comparison of the unsteadiness captured at and around the wave frequency, both measurements have been filtered to remove all content above 2 Hz. It can be seen that both the LDV (black line) and the probe (red line) capture the waves, and that they agree on the longer time-scales of unsteadiness in the tank. The higher frequencies indicate the presence of smaller turbulent flow structures, which will not be constant between the two locations. However, in periods when higher frequencies are absent, the agreement is good.

Figures 11(b) and (c) show the transverse and vertical velocities respectively. It can be seen that the magnitude of the fluctuations in transverse velocities agrees well between the LDV and

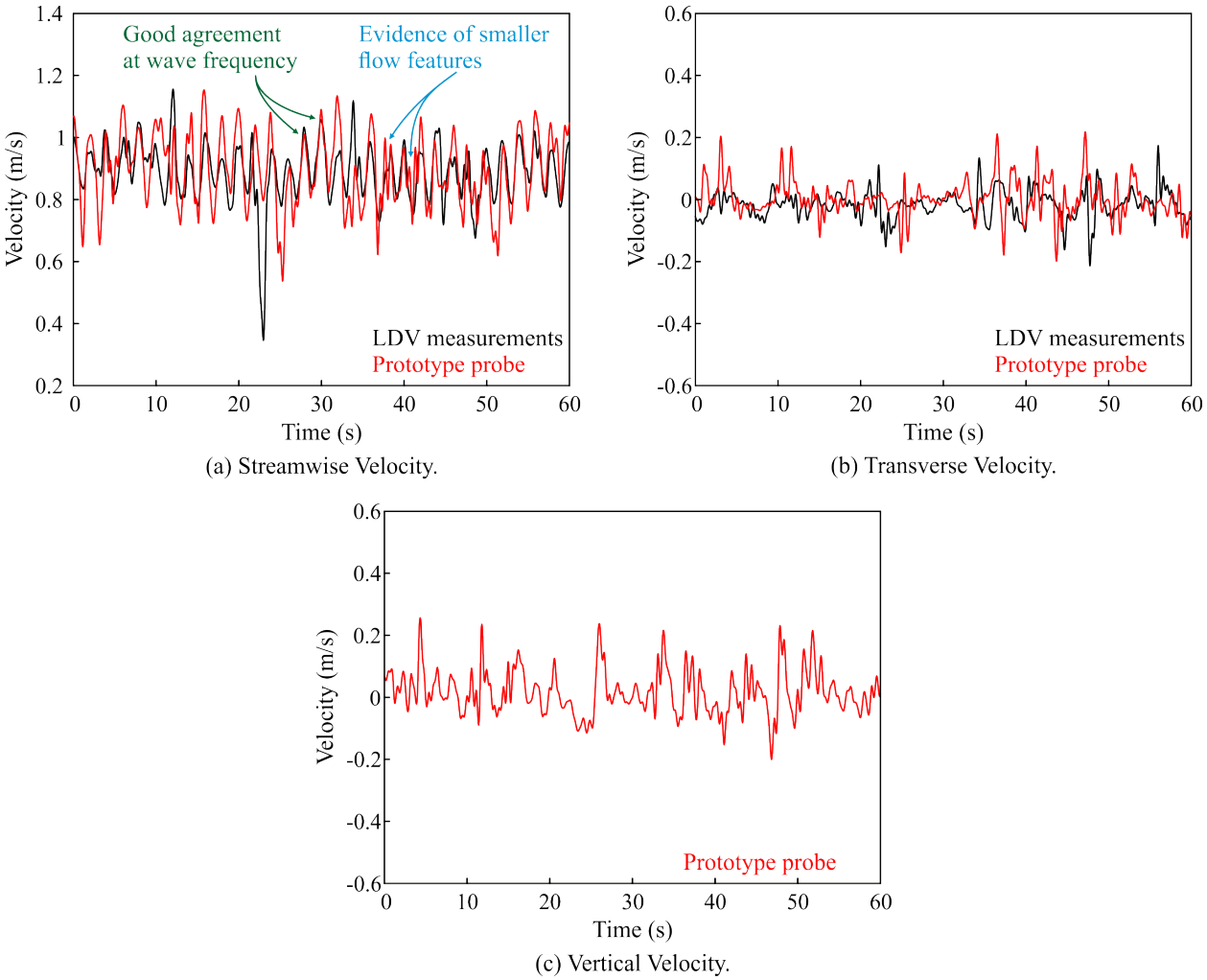

Fig. 11. Comparison of raw signals from LDV and prototype probe (0.8 m/s average flow speed, with waves at 0.5 Hz).

probe measurements. The LDV system was not set up to record the vertical velocity, but the vertical velocity recorded by the probe is shown in Fig. 11(c) for completeness.

Although it is not reasonable to expect that individual gusts are frozen as they convect from the LDV measurement location to the probe, the flow is likely to be statistically similar, if not homogeneous, between the two points. Thus, a more instructive way of comparing the data is through the power spectral densities of the signals, as shown in Fig. 12 for the transverse velocity component.

From Fig. 12, it can be seen that there is good agreement between devices and that the probe is able to resolve the 0.5 Hz waves clearly (Fig. 12(b)). The spectra agree well up to 20 Hz - the Nyquist frequency of the LDV data - and both spectra show a -5/3 decay as expected in the

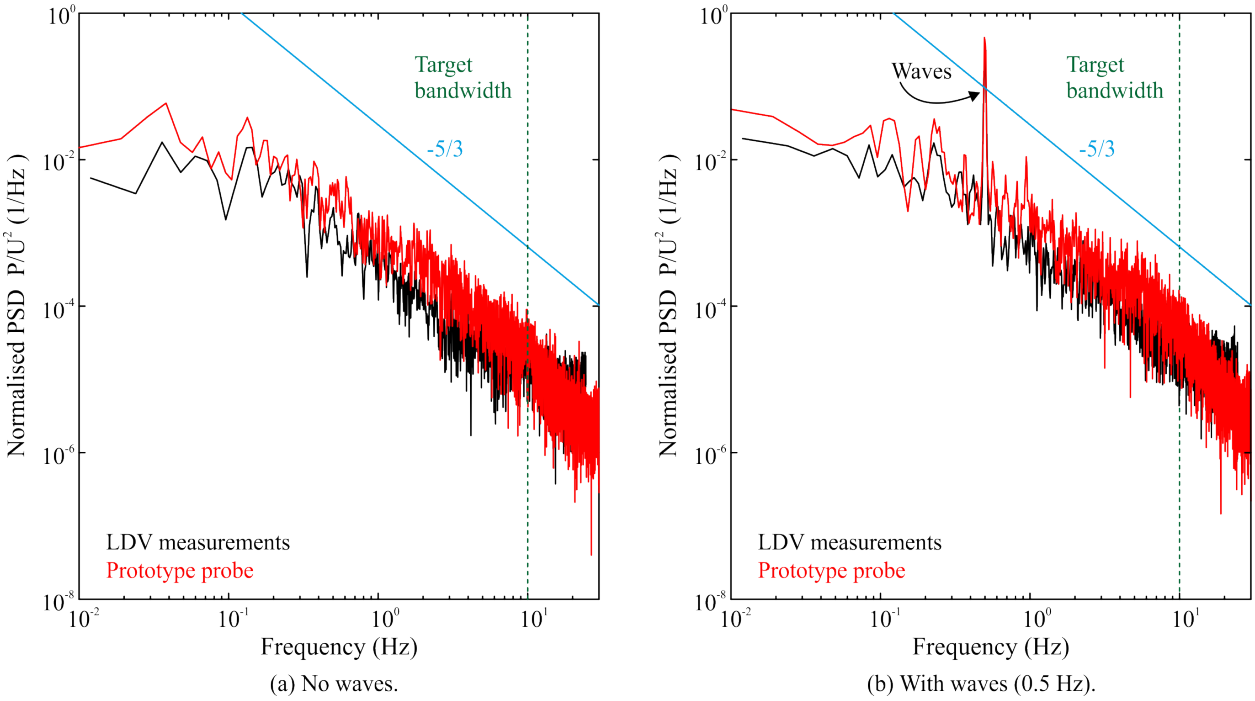

Fig. 12. Comparison of power spectral density of streamwise velocity from five-hole probe with LDV measurements with and without waves (0.8 m/s).

inertial subrange of a turbulent flow. There is a small offset between the probe and the LDV signals at low frequencies; this may be due to motion of the probe stem.

The power spectral densities of the signals in the transverse and vertical directions are shown in Fig. 13. It can be seen that, again, there is good agreement between the LDV and probe spectra. As with the streamwise spectra, the -5/3 roll-off is observed cleanly in all four plots.

As expected, the waves do not introduce any significant disturbance in the transverse direction, and neither device gives a spike at 0.5 Hz in Fig. 13(b). In the vertical direction, however, the waves would be expected to generate a substantial disturbance, and this is picked up clearly by both the probe and the LDV in Fig. 13(d) as a sharp spike at 0.5 Hz[2]. The magnitude of this spike is ten times smaller than that of the spike in the streamwise spectrum (Fig. 12(b)), and this explains why it is difficult to discern the 0.5 Hz fluctuations by eye in the vertical velocity trace in Fig. 11(c). The 0.5 Hz component is, however, clearly the major energy-containing frequency in the vertical direction and this is as expected.

[2]The LDV data shown here was acquired in a separate test to the probe data

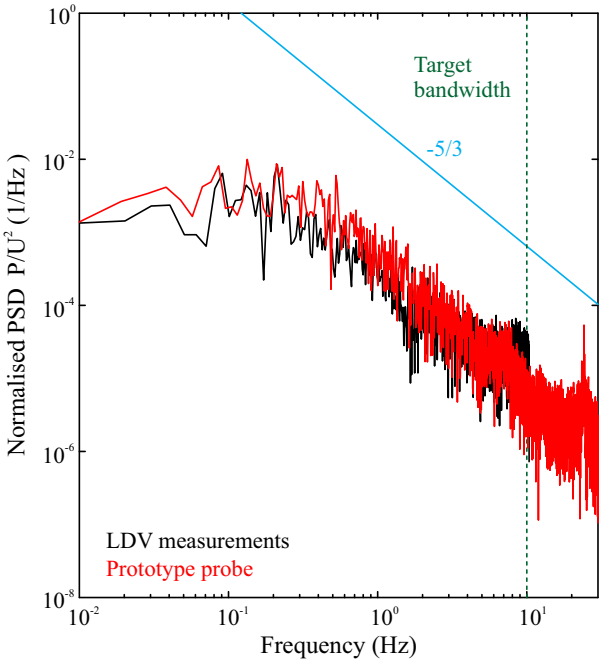

(a) Transverse direction, no waves.

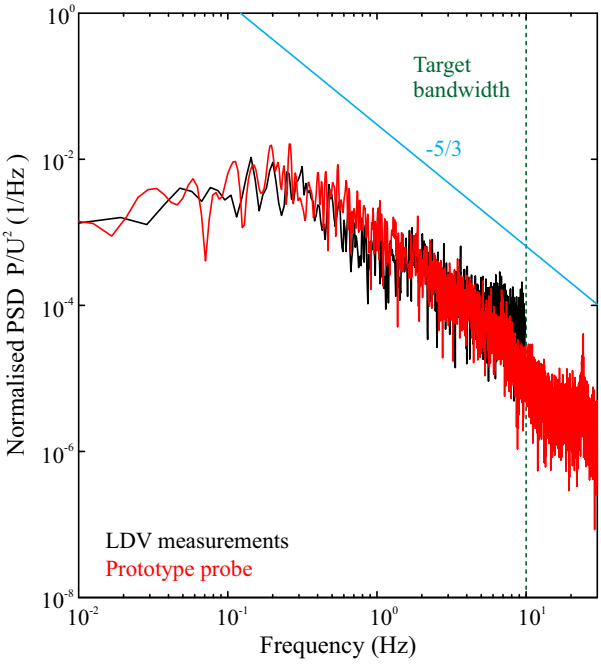

(b) Transverse direction, with waves (0.5 Hz).

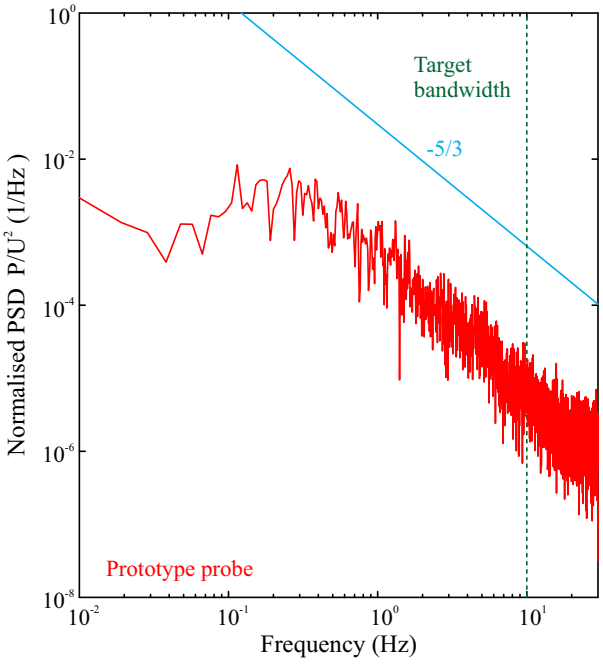

(a) Vertical direction, no waves.

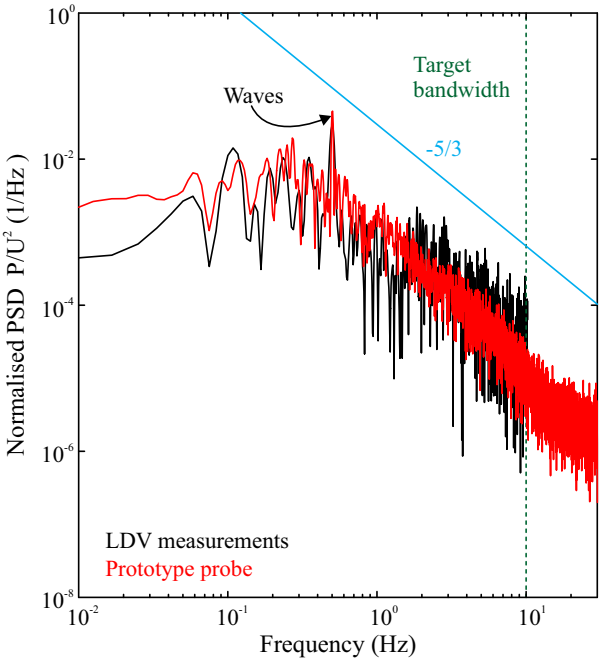

(b) Vertical direction, with waves (0.5 Hz).

Fig. 13. Comparison of transverse and vertical power spectral density from five-hole probe with LDV measurements with and without waves (0.8 m/s).

As well as the spectral content of the turbulent flow, it is useful to know the lengthscales of turbulence present. The standard technique for estimating turbulence lengthscales from single point measurements is to use the autocorrelation function and to define the 'integral timescale' as the area under the autocorrelation curve up to the first zero crossing. The integral lengthscale is then defined as the integral timescale multiplied by the bulk flow speed. This method is described in detail by Pope [14].

The autocorrelation of the streamwise data from both the LDV and the probe is plotted in Fig. 14 both in clean flow (Figs. 14(a) and (c)) and with waves (Figs. 14(b) and (d)). In each case, the upper plot shows the autocorrelation of data over 90 seconds, while the lower plot shows only the first five seconds, so that the agreement in the zero-crossing can be examined.

Looking at Fig. 14(a), it can be seen that the autocorrelation function for both data sets fluctuates over a period of about 25-30 seconds. This is approximately equal to the throughflow time of the tank and therefore could be linked to oscillations in the flow speed controller (which holds the flow nominally constant); long-timescale oscillations in the bulk flow speed are also apparent in the raw velocity traces in Fig 11.

Over the shorter period of time shown in Fig. 14(c), the agreement is good, though there is a significant difference in the zero crossing point, and the estimated turbulent lengthscale from the probe data is approximately 25% longer than that obtained from the LDV data. This difference may be due to the spatial offset between the LDV and the probe - although the spectra in Fig 12 are similar, the turbulence may be evolving between the two locations, and, if this is the case, the lengthscale would be expected to be longer at the downstream location (the probe) [15]. Alternatively, the difference in lengthscale in the streamwise direction could be due to probe motion, as postulated above.

Turning now to the autocorrelation data with the waves (Fig. 14(b) and (d)), it can be seen that the signal is dominated by a sinusoid with a period of approximately 2 seconds. This is to be expected: as shown by the spectra, the 0.5 Hz disturbance due to the waves contains substantially more energy than any other fluctuations in the flow and so the autocorrelation is dominated by this frequency. As with the spectra, the agreement between the LDV and the probe is good, with the zero-crossing point in almost exactly the same place in Fig. 14.

The autocorrelation of data in the transverse direction is compared in Fig. 15, with the same four plots shown as in Fig. 14. It can be seen the agreement between the LDV and the prototype probe is better in the transverse direction than the streamwise direction. The zero crossing point

is also closer to the y-axis, suggesting smaller disturbances are present in the transverse direction than in the streamwise direction. As with the spectra, comparing Figs. 15(c) and (d) it can be seen that the waves make very little difference to the flow in the transverse direction.

Finally, the autocorrelation of the probe data in the vertical direction is shown in Fig. 16 (LDV data is shown for the wave case in Fig. 16(b) and (d); this data is taken from a separate test). Without waves (Fig. 16(a) and(c)), it can be seen that the zero crossing occurs at a similar time to that observed in the transverse direction, suggesting eddies of a similar size. With waves (Fig. 16(b) and (d)), there is a 0.5 Hz sinusoidal pattern that emerges after the first zero crossing as with the streamwise data, and the agreement between the probe and LDV data is good. Again, this is in line with the spectra, which showed that the waves dominated the spectrum in the vertical direction.

From this anaylsis, it can be seen that the probe agrees with the LDV measurements and gives reliable information on the three-dimensional flow up to frequencies of 20 Hz. A frequency of 20 Hz corresponds to a 10 cm gust convecting with the flow - i.e. far smaller than the gusts that are important for tidal turbine design. This result, together with the low cost of the device, means that five-hole probes could be used to obtain high fidelity turbulence measurements at tidal power sites and thus give a vast improvement in the accuracy of unsteady load predictions.

XI. Future Improvements

The tests with the proof of concept device have shown that a five-hole probe can be used to capture unsteady flow features in a tidal channel flow. There are, however, some further improvements which need to be made in a production-ready device.

The main source of error in the measurements from the probe is due to drift in the zero offset of the pressure transducers. The use of higher quality transducers with a smaller pressure range would reduce this error. Alternatively, a cap-type device could be deployed to shield the probe from the flow while a zero reading was taken at regular intervals.

Secondly, two further pressure transducers could be added: an additional differential transducer placed out of the flow to measure the hydrostatic pressure gradient and an absolute sensor to give the hydrostatic pressure and therefore the depth of the probe.

Thirdly, a compass and tilt-meter would give the orientation of the probe and would enable its precise position and direction recorded while flow data was acquired. There is space in the probe head to house these devices.

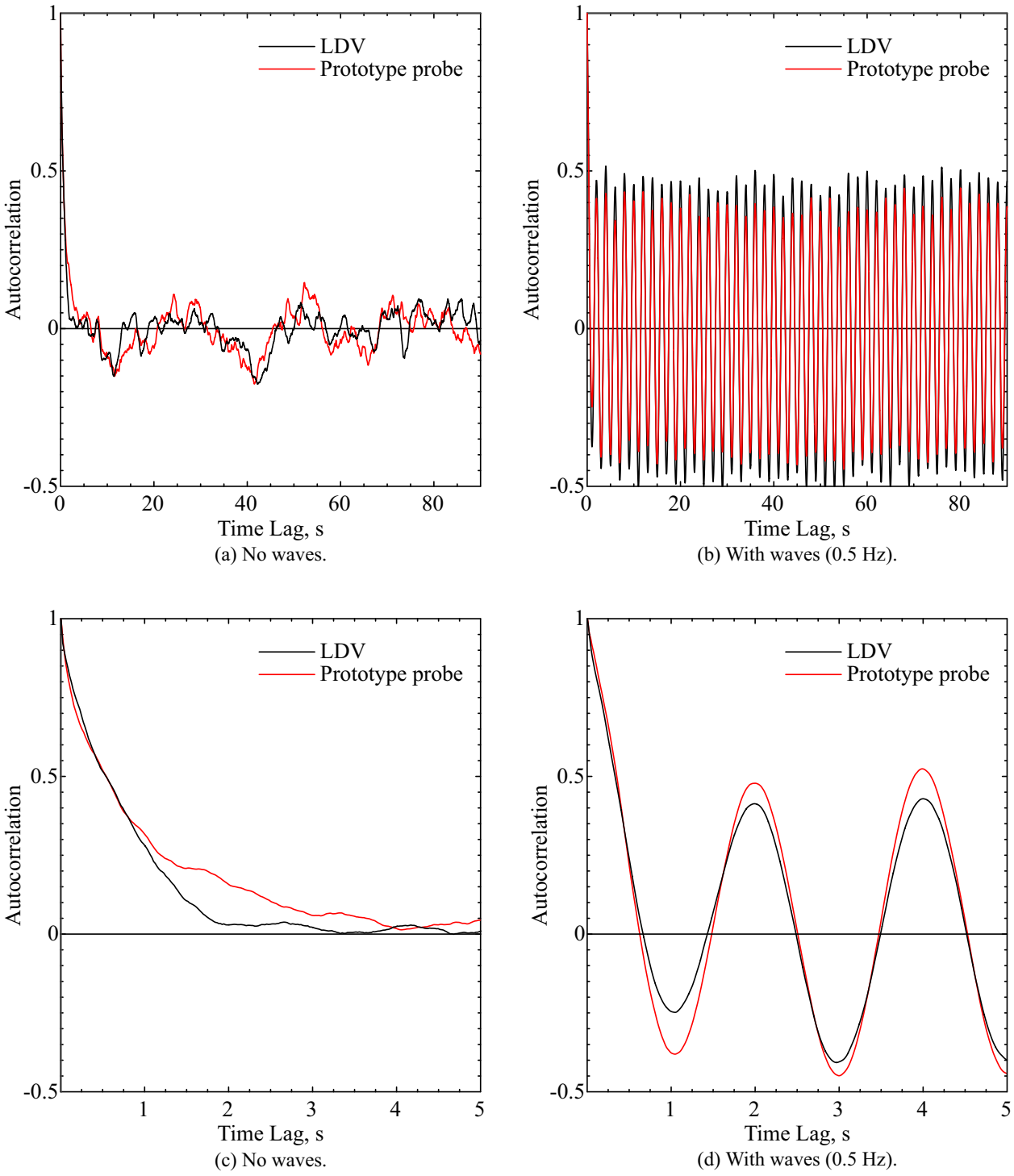

Fig. 14. Comparison of streamwise autocorrelation function from five-hole probe with LDV measurements with and without waves (0.8 m/s).

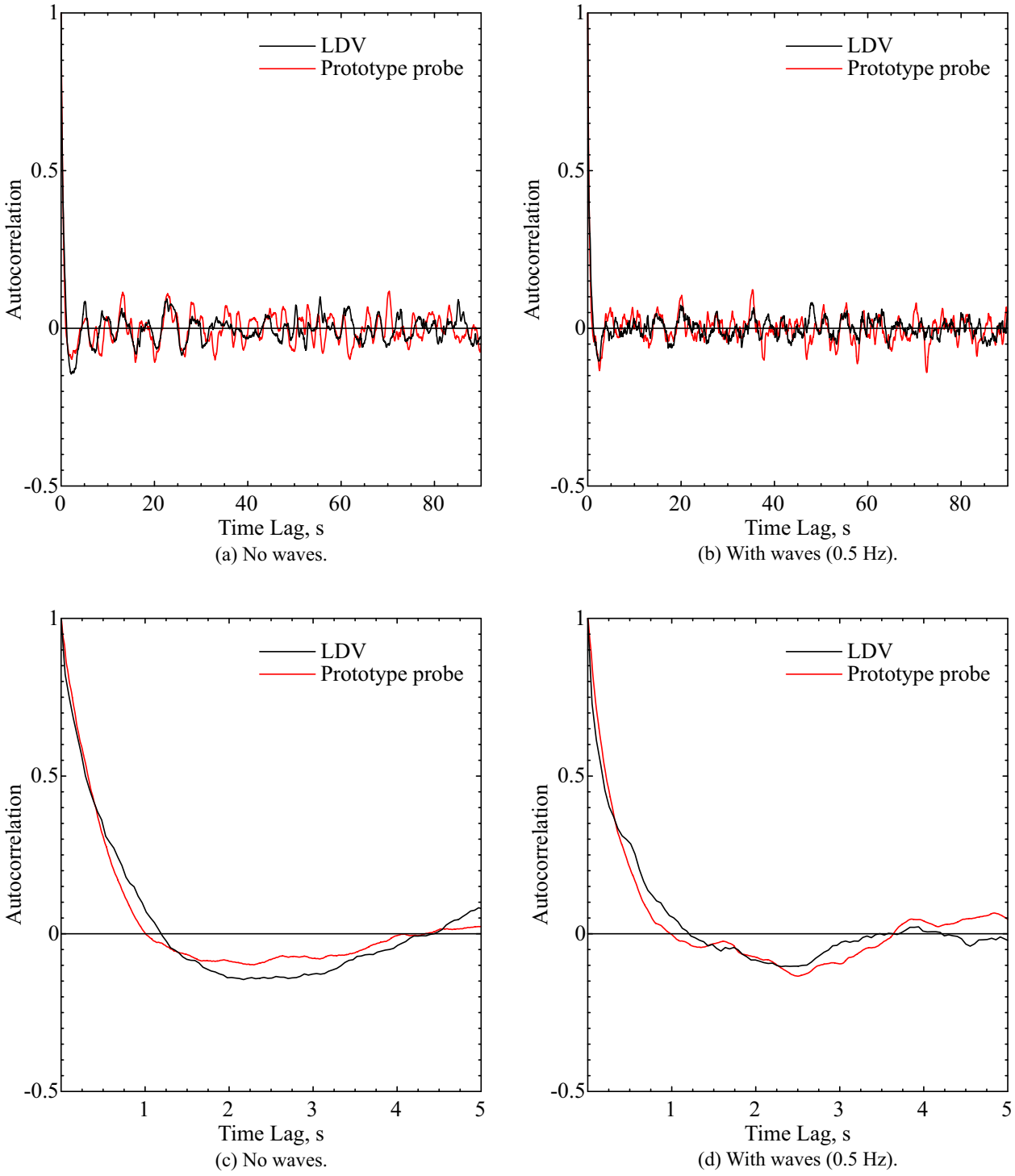

Fig. 15. Comparison of transverse autocorrelation function from five-hole probe with LDV measurements with and without waves (0.8 m/s).

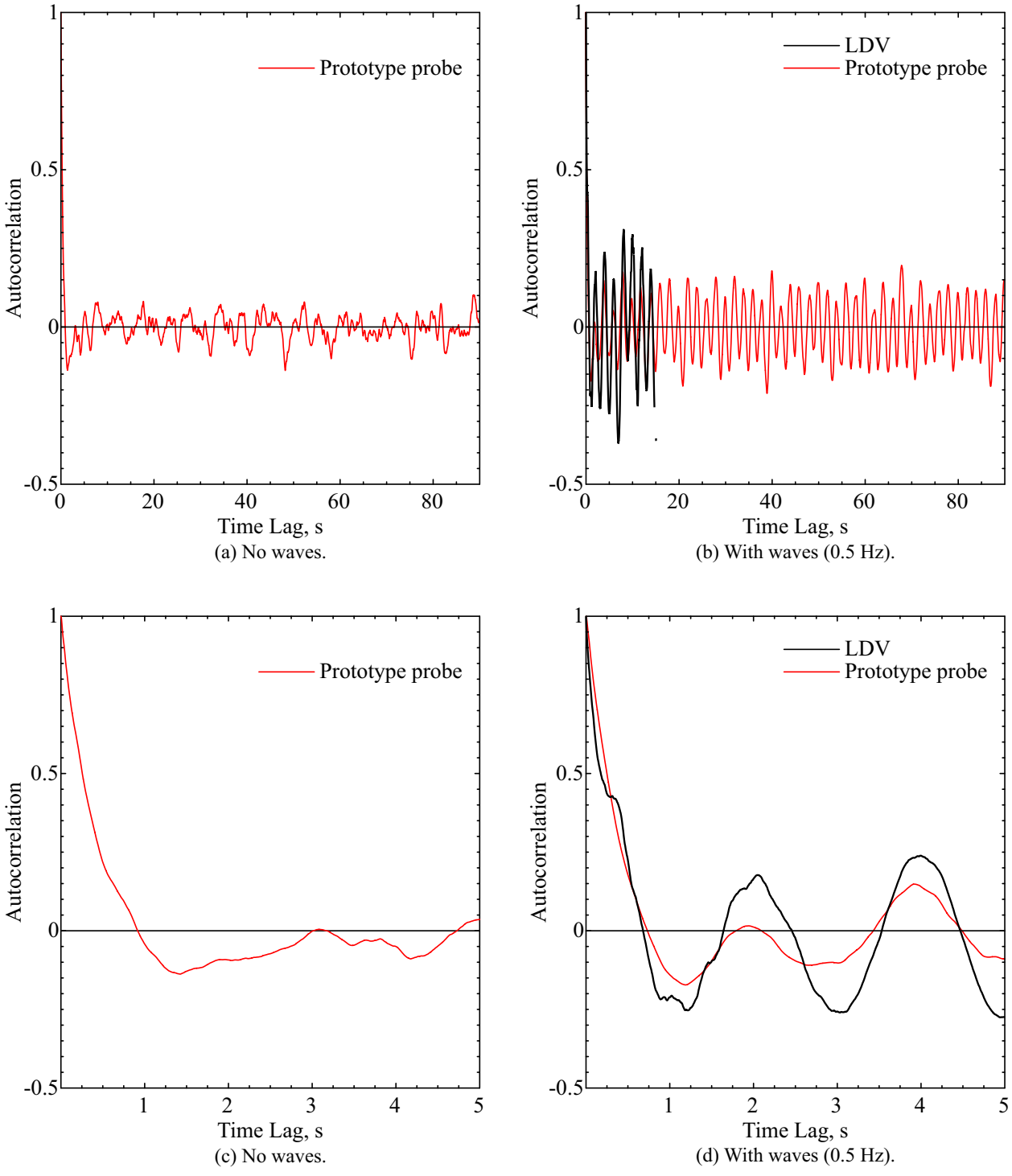

Fig. 16. Vertical autocorrelation function from five-hole probe with and without waves (0.8 m/s).

Fourthly, the calibration procedure must be refined and the generality of each step established. Due to the large scale of the probe relative to a typical aerospace device, geometric variations are likely to have a minimal effect on the calibration map [5]. This hypothesis needs to be verified in tests with several devices over a wider range of flow angles and speeds in order to produce a universal calibration map.

Finally, in terms of operability in the marine environment, the data acquisition and power must be integrated so that the probe operates remotely without a cable connecting to the surface. This would be achieved by placing a second PCB and a battery in the probe head, such that the device could be switched on and deployed to acquire data for a set period of time. The probe would then be retrieved and data transferred via an IP-68 rated data port. This connection would also allow monitoring and control in a laboratory environment.

XII. Conclusions

It has been shown that the unsteady five-hole probe represents a viable, low-cost means of obtaining turbulence measurements in tidal channels. The data provided by such a probe is of huge importance for tidal stream turbine development, where high-fidelity information on the inflow conditions across the whole site is needed in order for accurate fatigue life assessments to be made.

The primary difference between traditional five-hole probes used in air and the new marine probe demonstrated here is the novel differential connection which avoids the use of absolute pressure measurements or the need for a local reference pressure. The transducers are installed such that each measures the difference in pressure between one of the four side faces and the central hole. This, along with new calibration coefficients, allows the dynamic pressure to be measured accurately despite its small magnitude relative to the hydrostatic pressure.

A prototype probe has been built using off-the-shelf electronic components, with a bespoke amplifier for space reasons. It has been calibrated and tested in a flume tank at 1 m depth with mean flow from 0.4 m/s to 1.6 m/s.

The main source of error in the measurements from the probe is due to drift in the zero offset of the pressure transducers, which can cause errors of 5-10% in mean flow speed. If this drift can be accounted for, errors can be reduced to less than 5% of the mean velocity for flow speeds of 0.6 m/s and above. The use of higher quality transducers with a smaller pressure range would further reduce this error.

In tests alongside an LDV system, unsteady flow features, including waves, were captured accurately by the probe at frequencies of up to 20 Hz. This is well in excess of the frequencies required for tidal turbine fatigue life design calculations.

ACKNOWLEDGMENT

The authors would like to thank the staff at Ifremer for their assistance with testing, and Ivor Day and Chris Freeman for their technical help. An earlier version of this work was presented at the XXIII Biennial Symposium on Measuring Techniques in Turbomachinery, Stuttgart, 2016.

REFERENCES

[1] R. U. Guion and A. M. Young, "The frequency response of acoustic doppler current profilers: Spatiotemporal response and implications for tidal turbine site assessment," in *Oceans-St. John's, 2014*, pp. 1–10, IEEE, 2014.

[2] P. Duquesne, C. Deschênes, M. Iliescu, and G. Ciocan, "Calibration in a potential water jet of a five-hole pressure probe with embedded sensors for unsteady flow measurement," in *Fourth International Conference on Experimental Mechanics*, pp. 752217–752217, International Society for Optics and Photonics, 2009.

[3] P. Duquesne, G. D. Ciocan, V. Aeschlimann, A. Bombenger, and C. Deschênes, "Pressure probe with five embedded flush-mounted sensors: unsteady pressure and velocity measurements in hydraulic turbine model," *Experiments in fluids*, vol. 54, no. 1, p. 1425, 2013.

[4] M. J. Dunkley, *The aerodynamics of intermediate pressure turbines*. PhD thesis, University of Cambridge, 1998.

[5] B. F. Hall and T. Povey, "The oxford probe: an open access five-hole probe for aerodynamic measurements," *Measurement Science and Technology*, vol. 28, p. 035004, jan 2017.

[6] T. J. Dudzinski and L. N. Krause, "Flow-direction measurement with fixed-position probes," *NASA Technical Memorandum X-1904*, 1969.

[7] R. Dominy and H. Hodson, "An investigation of factors influencing the calibration of 5-hole probes for 3-d flow measurements," *Journal of Turbomachinery - Transactions of the ASME*, vol. 115, pp. 513–519, 1993.

[8] R. W. Ainsworth, J. L. Allen, and J. J. M. Batt, "The development of fast response aerodynamic probes for flow measurements in turbomachinery," in *ASME 1994 International Gas Turbine and Aeroengine Congress and Exposition*, pp. V005T15A002–V005T15A002, American Society of Mechanical Engineers, 1994.

[9] B. Gaurier, P. Davies, A. Deuff, and G. Germain, "Flume tank characterization of marine current turbine blade behaviour under current and wave loading," *Renewable Energy*, vol. 59, pp. 1 – 12, 2013.

[10] O. D. Medina, F. G. Schmitt, R. Calif, G. Germain, and B. Gaurier, "Turbulence analysis and multiscale correlations between synchronized flow velocity and marine turbine power production," *Renewable Energy*, vol. 112, pp. 314–327, 2017.

[11] G. Zilliac, "Modelling, calibration, and error analysis of seven-hole pressure probes," *Experiments in Fluids*, vol. 14, no. 1-2, pp. 104–120, 1993.

[12] C. Chondrokostas, R. Willinger, and S. Tsangaris, *Calibration of pneumatic five-hole probes in the free-jet wind tunnel*. PhD thesis, Technical University of Vienna, 2005.

[13] C. Tropea and A. L. Yarin, *Springer handbook of experimental fluid mechanics*, vol. 1. Springer Science & Business Media, 2007.

[14] S. B. Pope, *Turbulent Flows*. Cambridge University Press, 2000.

[15] P. Roach, "The generation of nearly isotropic turbulence by means of grids," *International Journal of Heat and Fluid Flow*, vol. 8, no. 2, pp. 82–92, 1987.